Thermoanalytical, Spectroscopic and DFT Studies of Heavy Trivalent Lanthanides and Yttrium(III) with Oxamate as Ligand

Flávio Junior Caires[a]*, Wilhan Donizete Gonçalves Nunes[b], Caroline Gaglieri[a], André Luiz

Carneiro Soares do Nascimento[b], José Augusto Teixeira[b], Geórgia Alvim Coelho Zangaro[b],

Oswaldo Treu-Filho[b], Massao Ionashiro[b]

[a] Faculdade de Ciências, Universidade Estadual Paulista Júlio de Mesquita Filho - UNESP, Bauru, SP, Brazil
[b] Instituto de Química, Universidade Estadual Paulista Júlio de Mesquita Filho - UNESP, Araraquara, SP, Brazil

Solid-state $LnL_3 \cdot nH_2O$ complexes, where Ln stands for trivalent lanthanides (Tb to Lu) or yttrium(III) and L is oxamate ($NH_2COCO_2^-$), have been synthesized. The characterization of the complexes was performed by using elemental analysis (EA), complexometric titration with EDTA, thermoanalytical techniques such as simultaneous thermogravimetry and differential scanning calorimetry (TG-DSC), evolved gas analysis (TG-FTIR), infrared spectroscopy (IR) and powder X-ray diffraction (XRPD). The results provided information about thermal behavior, crystallinity, stoichiometry, coordination sites, as well as the products released during thermal degradation of the complexes studied. Theoretical calculation of yttrium oxamate, as representative of all complexes was performed using density functional theory (DFT) for studying the molecular structure and vibrational spectrum of the investigated molecule in the ground state. The optimized geometrical parameters and theoretical vibrational spectrum obtained by DFT calculations are in good agreement with the experimental results.

1. Introduction

The oxamic acid is composed of carboxyl group and primary amide group and molecular formula $C_2H_3NO_3$. It has molar mass of 89.05 g mol^{-1}, odorless, sublimates and melts partly around 140 ºC and it is found as a white solid.

The oxamic acid is well known as a versatile ligand and can act as di, tri or tetradentate (bridging) regarding its coordination modes, or as mono or dianion, when the charge is taken into account. When treated as a monoanion, it can coordinate by two of its oxygen atoms, forming a five-membered chelate ring, or by one oxygen atom (from the carboxylate group) and the nitrogen (amide group). Still as a monoanion it can act as a monodentate ligand using one oxygen atom from the carboxylic group; or as a tridentate ligand using all of its oxygen atoms. In the dianion form, when it loses of its ionisable hydrogens, it can act as a chelate bidentate or bridging ligand, and also as bridging tetradentate ligand in binuclear complexes, which also can contain other multidentate chelate ligands[1].

A few studies about complexes involving lanthanides and oxamic acid are found in the literature. Two of them describe the synthesis, the determination of physical properties, spectroscopic studies and thermal behavior of lanthanide (III) oxamates[2,3]. The others reported the crystal structure determination of the oxamate praseodymium, neodymium, and holmium[1,4,5].

The present paper reports the preparation of solid-state complexes of heavy trivalent lanthanides with oxamate and the investigation by means of complexometry, elemental analysis, simultaneous thermogravimetry and differential scanning calorimetry (TG-DSC), TG-DSC coupled to FTIR, powder X-ray diffraction (PXRD) and infrared spectroscopy (FTIR). DFT calculations were performed in order to compare and support the experimental results. This work is primarily a continuation and extension of the reported study on the thermal behavior of light trivalent lanthanide oxamates[6].

2. Experimental

The oxamic acid, $H_2NCOCOOH$, with 99% purity was obtained from Sigma and used as received.

The basic carbonates of heavy trivalent lanthanides (Tb to Lu) and yttrium (III) were prepared following the procedure described in the literature[6].

Solid-state heavy trivalent lanthanide and yttrium oxamates were prepared following the literature method[6]:

* e-mail: caires.flavio@fc.unesp.br

Under stirring, slight excess of the corresponding metal basic carbonate was added to 50 mL of an aqueous suspension of oxamic acid 0.15 mol L^{-1}.

For the solid-state complexes, metal ions, hydration water, and oxamate contents were determined from TG curves. The metal ions were also determined by complexometry with standard EDTA solution after igniting the complexes to the respective oxides and their dissolution in hydrochloric acid solution[6].

Carbon, hydrogen and nitrogen contents were determined by microanalytical procedures, with a CHN Elemental Analyzer from Perkin Elmer, model 2400.

Simultaneous TG-DSC curves were obtained in a Mettler Toledo TG-DSC 1 thermal analysis system. The purge gas was dry air with flow of 50 mL min^{-1}. Heating rate of 10 ºC min^{-1} was used, with samples weighing about 7.0 mg. Alumina crucibles were used for recording the TG-DSC curves.

The evolved gas analysis (EGA) was performed using a Mettler TG-DSC thermogravimetric analyzer coupled to a Nicolet FTIR spectrophotometer with gas cell and DTGS KBr detector. The TG furnace and heated gas cell (250 ºC) were coupled through a heated (225 ºC) 120 cm stainless steel line transfer with diameter of 3.0 mm, both purged with dry air (50 mL min^{-1}). The FTIR spectra were recorded with 16 scans per spectrum at a resolution of 4 cm^{-1}.

X-ray powder diffraction (XRPD) data were obtained by using a Siemens D-5000 X-Ray Diffractometer employing CuKα radiation ($\lambda = 1.541$ Å) and setting of 40 kV and 20 mA.

The attenuate total reflectance infrared spectra of sodium oxamate as well as of its metal-ion complexes were recorded using a Nicolet iS10 FTIR spectrophotometer, using an ATR accessory with a Ge window. The FTIR spectra were recorded with 32 scans per spectrum at resolution of 4 cm^{-1}.

2.1. Computational strategy

In this study, the quantum chemical approach employed to determine the molecular structures was Becke's three parameter hybrid theory[7] using the Lee-Yang-Par (LYP) correlation functional[8], and the basis sets used for calculations were: 4s for H (^{2}S)[9], [5s4p] for C (^{3}P), N (^{4}S) and O (^{3}P) (9), and [14s7p7d] for Y (^{2}D)[10]. The diffuse functions for the yttrium atom (^{2}D) were calculated according to the procedure described by Teu-Filho et al.[9] and these values are: αs = 0.007007235, αp = 0.991840315, αd = 0.008880095. Full details about the wave function developed in this work are available upon request to the e-mail address: oswaldo.treu.filho@gmail.com.

In order to better describe the properties of the complex in the implementation of the calculations, it was necessary to include polarization functions [9-11] for all atoms of the complex. The polarization functions are: αp = 0.33353749 for H (^{2}S), αd = 0.72760279, αd = 0.35416230 αd = 0.36059494 for C (^{3}P), N (^{4}S) and O (^{3}P), respectively, and αf = 0.394056689 for

Y (^{2}D) atoms. The role of a basis set is crucial in theoretical studies of metal complexes, since the description of the metal configuration in the complex differs from the neutral state. The performed molecular calculations in this study were made using the Gaussian 09 routine[12].

The theoretical infrared spectrum was calculated using a harmonic field[13] based on C$_1$ symmetry (electronic state ^{1}A). Frequency values (not scaled), relative intensities, assignments, and description of vibrational modes are presented. The geometry optimization was computed using the optimized algorithm of Berny[14] and the calculations of vibrational frequencies were also implemented to determine if the optimized geometry constitutes minimum or saddle points . The principal infrared active fundamental mode assignments and descriptions were done by the GaussView 5.0.2 W graphics routine[15].

3. Results and Discussion

3.1. Analytical results

The analytical and thermoanalytical (TG) results for the synthesized complexes are shown in Table 1. The analytical results are in good agreement with the thermoanalytical ones, evidencing that the complexes were obtained in a high degree of purity. From the results, it was possible to establish the stoichiometry of the complexes, which is in agreement with the general formula: Ln(L)$_3$·nH$_2$O, where Ln represents heavy trivalent lanthanides, L is oxamate and n = 1 (Dy, Ho, Y); 1.25 (Er); 1.5 (Tb and Lu); 2 (Tm) and 2.5 (Yb).

3.2. Thermal analysis (TG-DSC and EGA)

The simultaneous TG-DSC curves of the complexes are shown in Figure 1. In all complexes, the TG curves show mass losses in four consecutive and/or overlapping steps, although the DSC curves show that the thermal decomposition occurs with a large number of consecutive and/or simultaneous steps and through a more complex pathway than that observed in the TG curves. The mass losses corresponding to endothermic peaks are attributed to the dehydration or thermal decomposition and the exothermic ones to the oxidation of the organic matter and/or of the gaseous products evolved during the thermal decomposition.

The thermal decomposition reaction interval (I) from anhydrous complexes and final temperature of thermal decomposition (II) as shown by the curves TG-DSC depends on the nature of the metal ion and they follow the order:

(I) Ho > Y = Er = Dy > Lu > Tm > Yb > Tb
**(II) Er > Ho > Lu = Y > Dy > Tm > Yb > Tb**
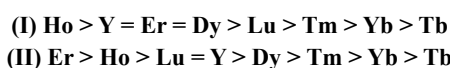
A great similarity is observed in the profiles of the TG curves, except for the terbium complex. On the other hand,

Table 1. Analytical and thermoanalytical (TG) data for $Ln(L)_3 \cdot nH_2O$ complexes.

Complexes	Ln (oxide)/ %		L (lost)/ %		H_2O/ %		C/ %		H/ %		N/ %		Final Residue
	Calc.	EDTA	TG	Calc.	TG	Calc.	TG	Calc.	EA	Calc.	EA	Calc.	EA	
$Tb(L)_3 \cdot 1.5H_2O$	39.77	39.50	39.77	52.21	52.64	6.01	5.57	16.01	16.01	2.02	2.02	9.34	9.34	Tb_4O_7
$Dy(L)_3 \cdot 1H_2O$	41.95	41.50	41.02	54.00	54.67	4.05	4.31	16.21	16.47	1.82	1.85	9.45	9.61	Dy_2O_3
$Ho(L)_3 \cdot 1H_2O$	42.26	42.06	42.31	53.71	53.81	4.03	3.88	16.12	16.10	1.81	1.81	9.40	9.39	Ho_2O_3
$Er(L)_3 \cdot 1.25H_2O$	42.14	41.87	41.36	52.90	53.52	5.90	5.12	15.88	16.09	1.89	1.92	9.26	9.38	Er_2O_3
$Tm(L)_3 \cdot 2H_2O$	41.13	40.97	41.18	51.19	51.53	7.68	7.29	15.36	15.35	2.15	2.15	8.96	8.95	Tm_2O_3
$Yb(L)_3 \cdot 2.5H_2O$	40.86	40.39	40.51	49.79	50.37	9.34	9.12	14.94	15.03	2.30	2.32	8.72	8.77	Yb_2O_3
$Lu(L)_3 \cdot 1.5H_2O$	42.69	42.40	42.83	51.52	51.39	5.80	5.78	15.46	15.42	1.95	1.95	9.02	8.99	Lu_2O_3
$Y(L)_3 \cdot 1H_2O$	30.43	30.20	30.46	64.71	64.64	4.86	4.90	19.42	19.41	2.18	2.18	11.33	11.32	Y_2O_3

L: oxamate.
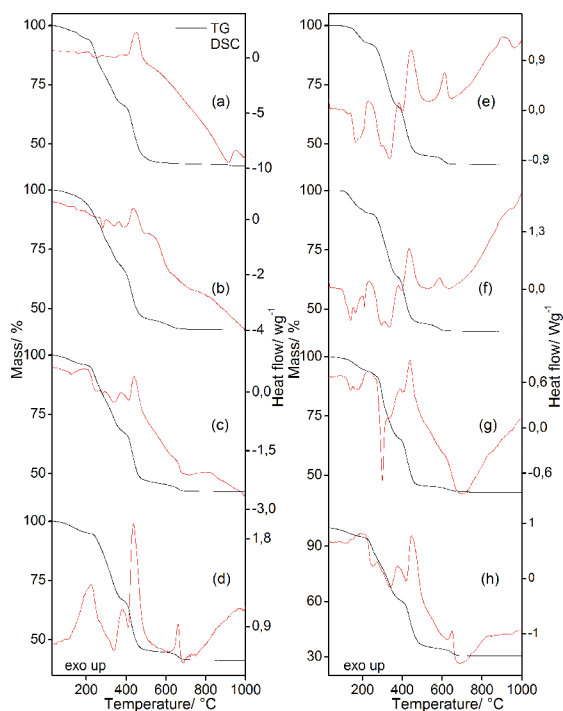
Figure 1. Simultaneous TG-DSC curves of the complexes: (a) $Tb(L)_3 \cdot 1.5H_2O$, (b) $Dy(L)_3 \cdot 1H_2O$, (c) $Ho(L)_3 \cdot 1H_2O$, (d) $Er(L)_3 \cdot 1.25H_2O$, (e) $Tm(L)_3 \cdot 2H_2O$, (f) $Yb(L)_3 \cdot 2.5H_2O$, (g) $Lu(L)_3 \cdot 1.5H_2O$ and (h) $Y(L)_3 \cdot 1H_2O$.

the profiles of the DSC curves show great similarity for two sets of complexes (Tb, Dy, Ho and Tm, Yb) and particular ones for the other complexes (Er, Lu and Y), as also observed in all DSC curves of the trivalent light lanthanide oxamates[6]. Thus, the features of each complex are discussed based on their similar thermal profiles from TG curves.

Terbium complex

The TG-DSC curves of the complex are shown in Figure 1 (a). These curves show mass losses in four steps and thermal events corresponding to these losses. The first mass loss that occurs through a slow process corresponding to an endothermic peak is attributed to dehydration.

The thermal decomposition of the anhydrous complexes occurs in three steps immediately after the dehydration and the first two mass losses corresponding to endothermic peaks are attributed to the thermal decomposition and an exothermic peak due to the oxidation of organic matter and/or of the gaseous products evolved in the thermal decomposition, with the formation of terbium oxide, Tb_4O_7. The last mass loss between 900 and 940 ºC corresponding to an endothermic peak at 910 ºC is attributed to reduction reaction of Tb_4O_7 to Tb_2O_3, as already observed in other studies[16,17].

Dysprosium to lutetium and yttrium

The TG-DSC curves of these complexes are shown in Figure 1 (b - h). These curves also show mass losses in four steps and thermal events corresponding to these losses. The first mass loss that occurs slowly corresponding to an endothermic peak (Ho, Tm, Y), and two (Dy) or three endothermic peak (Yb, Lu) is attributed to dehydration.

After the dehydration, the thermal decomposition of the anhydrous complexes occurs in three steps. The first two - corresponding to endothermic peaks - are attributed to the thermal decomposition, and the last - associated with an exothermic peak - is attributed to the oxidation of organic matter and/or of the gaseous products evolved in the thermal decomposition, with the formation of a mixture of carbonaceous residue and a derivative of carbonate. Tests with hydrochloric acid solution on samples heated up to the temperature of formation of this mixture, as indicated by the corresponding TG-DSC curves confirmed the formation of carbonate by the evolution of CO_2 and the presence of carbonaceous residue. The formation of carbonaceous residue and of derivative of carbonate had already been observed in the thermal decomposition of some light trivalent lanthanide oxamates[6] and other lanthanide complexes[18,19].

The last mass loss corresponding to no thermal events (Dy, Lu), small endothermic peak (Ho) or exothermic peaks (Er, Tm, Yb, Y) is attributed to oxidation of carbonaceous residue (exo) and thermal decomposition of the derivative of carbonate (endo). Calculations based on the mass losses

observed in the TG curves are in agreement with the formation of the respective oxides, Ln_2O_3 (Ln = Tb to Lu and Y) and confirmed by X-ray powder patterns.

In spite of the similarity in the TG profiles of these complexes, the temperature ranges (θ), mass losses (m) and temperature peaks (p) observed in each steps of the TG-DSC curves are characteristic of each complex, and for that reason this information is provided in Table 2.

EGA

The Gram-Schmidt curves (GS) and the IR spectra of the gaseous products released during the thermal decomposition of the thulium complex, as representative of all the complexes, are presented in Figure 2. In general, GS curves are very similar to DTG curves (supplementary material), and thus their profiles can be correlated to the number of mass loss steps. The differences that may arise between them are probably due to the fact that GS curve profile is related to the molar absorption coefficient of the molecules of gases while the DTG curve is related to mass variation. The GS curve shows four maximum-intensity regions, and the second consisting

of two maximum values (two peaks). This suggests that the thermal decomposition takes place in at least four steps, and can be confirmed by inspecting the second mass loss in the TG curve, that is formed by at least two overlapping steps, as confirmed by the DTG curve. In addition, the GS curve shows that all steps are superposed, in agreement with the TG/DTG-DSC curves.

The gases released during the thermal decomposition were identified based on FTIR reference spectra available in the spectrometer's software database and analysis of the frequencies of the vibrational modes. The spectra obtained up to approximately 200 ºC show characteristic bands of water vapor (ν O-H in the range 4000-3400 cm^{-1} and δ O-H in the range of 2060 to 1260 cm^{-1}) attributed to dehydration of the complexes, as indicated by curves TG-DSC. Above 200 ºC, the main gas species identified were ammonia (characteristic bands at 3334 cm^{-1} (νNH_3) and 1626, 966 cm^{-1} (δNH_3), CO_2 (characteristic absorption bands at 2355 and 2311 cm^{-1} (νCO_2) and 669 cm^{-1} (δ CO_2); CO (characteristic band at 2154 cm^{-1} (ν CO)); N_2O (characteristic band at 2220 cm^{-1}), HCN (bands at 3300 cm-1 (ν C-H and 712 cm^{-1} (δ HCN)).

Table 2. Temperature ranges (θ), mass losses (Δm) and peak temperatures (Tp) observed for each step of TG-DSC curves of the complexes.

Complexes		TG-DSC Steps				Δm_{Total}
		First	Second	Third	Fourth	
Tb(L)$_3$·1.5H$_2$O	θ/ ºC	55 - 205	205 - 370	370 - 600	900 - 940	
	T$_p$/ ºC	170↓	250↓, 340↓	450↑	910↓	59.36
	Δm/ %	5.57	27.06	25.36	1.37	
Dy(L)$_3$·1H$_2$O	θ/ ºC	55 - 190	190 - 360	360 - 530	530 - 670	
	T$_p$/ ºC	120↓sm, 160↓sm, 175↓sm	285↓, 340↓	435↑	-	58.98
	Δm/ %	4.31	26.14	24.36	4.17	
Ho(L)$_3$·1H$_2$O	θ/ ºC	55 - 190	190 - 370	370 - 500	500 - 690	
	T$_p$/ ºC	132↓, 155↓sh	250↓, 285↓sh, 340↓	415↓, 440↑	680↓	57.69
	Δm/ %	3.88	27.11	21.92	4.78	
Er(L)$_3$·1.25H$_2$O	θ/ ºC	55 - 220	220 - 385	385 - 530	530 - 700	
	T$_p$/ ºC	-	340↓	410↓, 435↑	660↑	58.64
	Δm/ %	5.12	28.21	21.42	3.89	
Tm(L)$_3$·2H$_2$O	θ/ ºC	100 - 215	215 - 370	370 - 500	500 - 630	
	T$_p$/ ºC	125↓, 162↓, 180↓sh	330↓	390↓, 435↑	605↑	58.82
	Δm/ %	7.29	26.95	20.52	4.06	
Yb(L)$_3$·2.5H$_2$O	θ/ ºC	100 - 210	210 - 365	365 - 470	470 - 620	
	T$_p$/ ºC	140↓, 160↓, 205↓	290↓, 325↓	390↓, 425↑	580↑	59,49
	Δm/ %	9.12	27.08	19.38	3.91	
Lu(L)$_3$·1.5H$_2$O	θ/ ºC	55 - 220	220 - 385	385 - 470	470 - 680	
	T$_p$/ ºC	145↓, 170↓, 185↓	262↓sh, 300↓, 330↓sh	400↓, 440↑	-	57.17
	Δm/ %	5.78	28.69	19.30	3.40	
Y(L)$_3$·1H$_2$O	θ/ ºC	50 - 200	200 - 370	370 - 510	510 - 680	
	T$_p$/ ºC	130↓, 155↓ sh	260↓, 295↓sh, 340↓	420↓, 445↑	640↑	69.54
	Δm/ %	4.90	32.62	26.52	5.50	

L = oxamate; sm = small; sh = shoulder; ↓ = endothermic; ↑ = exothermic.
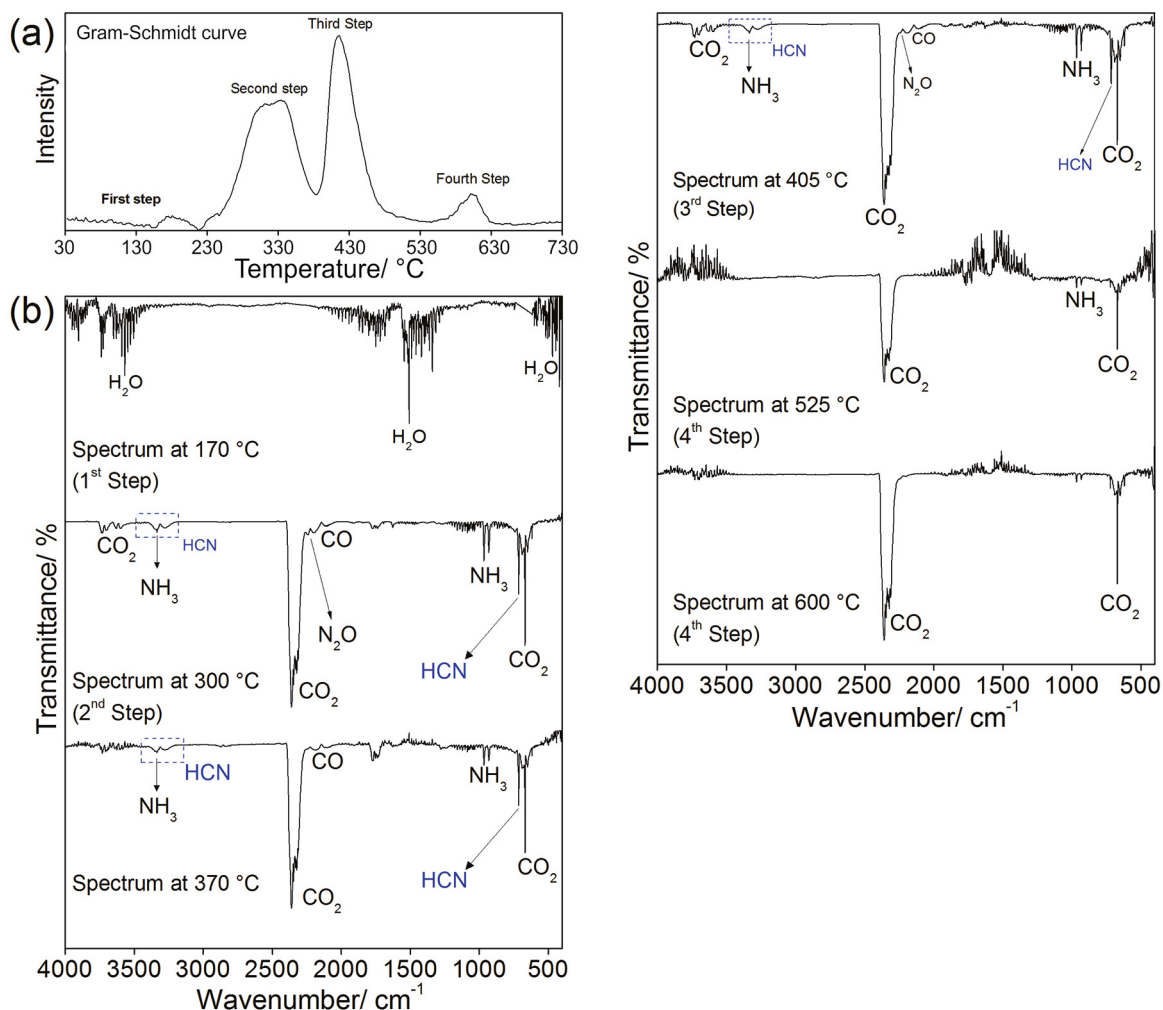
Figure 2. (a) Gram–Schmidt curve and (b) IR spectra of gaseous products evolved during the thermal decomposition of the yttrium complex.

Spectrum obtained at 600 ºC shows characteristic bands of CO_2 molecule, in accordance with the decomposition of the carbonate derivative with formation of thulium oxide.

3.3. Molecular modeling and vibrational spectroscopy in the infrared region

The calculated geometries are shown in Figure 3. Theoretical calculations showed that the structure in Fig 3a (isomer 1) is 10.90, 22.24 and 34.86 kcal mol^{-1} more stable than the structures 3b (isomer 2), 3c (isomer 3) and 3d (isomer 4) respectively. These theoretical results suggest that the ligand oxamate coordinates to the metal center in a bidentate mode, by one of the oxygen atoms from the carboxylate group and the oxygen atom of the amide group forming a chelate five membered ring (Figure 3a), agreeing with the structure determined by single crystal X-ray diffraction[1]. The structural parameters obtained from the most stable structure are shown in the supplemental material (Table S1).
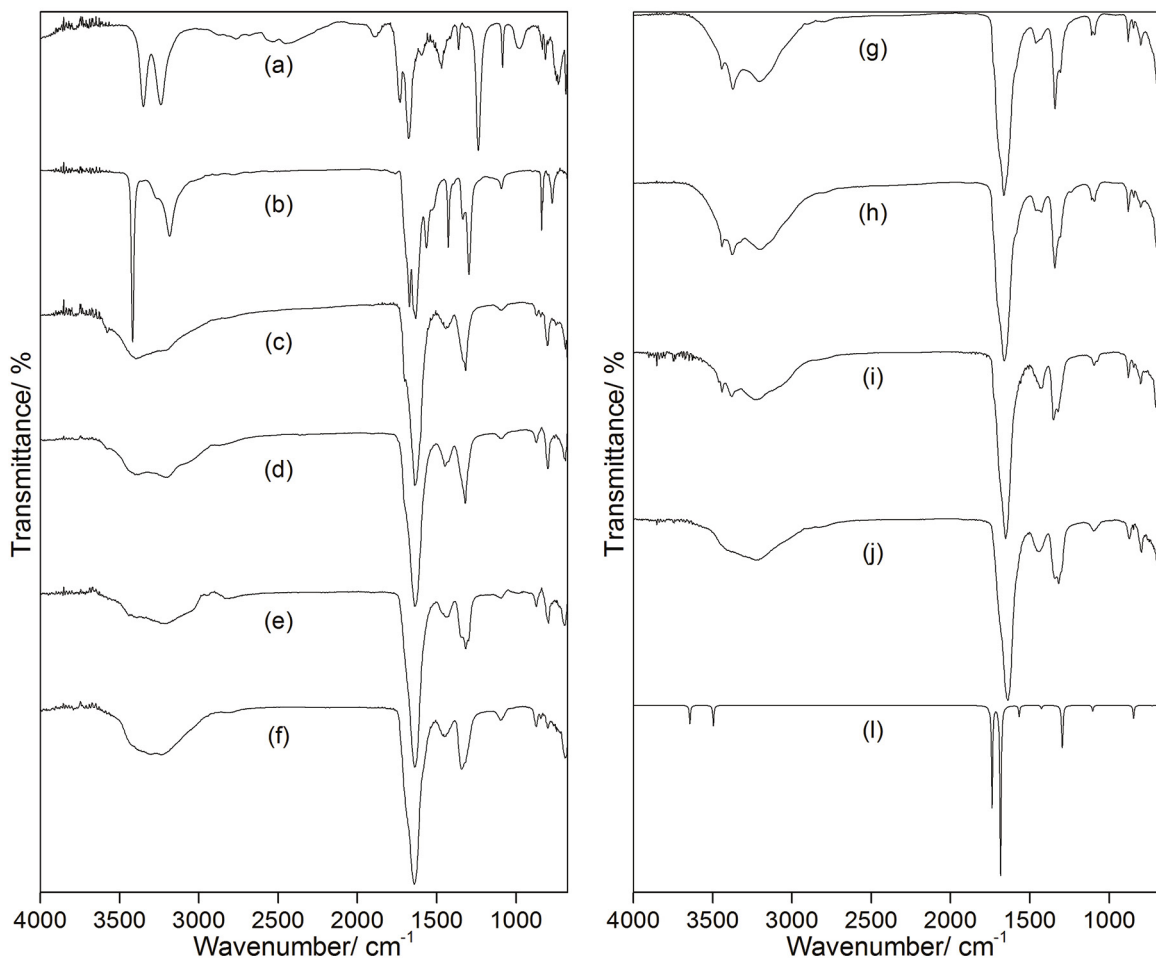
The vibrational spectra in the infrared region of the oxamic acid, sodium oxamate, lanthanide complex and the calculated from the more stable structure of the yttrium complex are shown in Figure 4.

The assignments were made based on theoretical calculations and also on the existing literature[20,21] and are presented in Table 3.

Comparative analysis of some bands observed in the experimental and theoretical spectra shows: (i) a band at 1683 cm^{-1}, while the theoretical result shows the corresponding peak at 1744 cm^{-1} with 3.62% discrepancy; (ii) a very strong band at 1638 cm^{-1}, while the theoretical spectrum shows the band corresponding to 1689 cm^{-1}, resulting in a 3.11% discrepancy; and (iii) a strong band at 1318 cm^{-1}, while the theoretical result shows the corresponding band in at 1295 cm^{-1}, a 1.75% discrepancy. The theoretical results are in very good agreement with the experimental data suggesting that the structure shown in Figure 3a can represent or be close to the real structure.
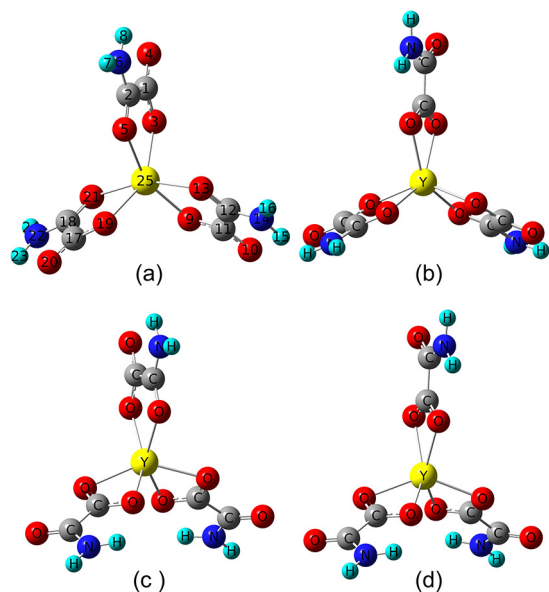
Figure 3. Optimized geometric structure of the Y(L)3: (a) Isomer 1 (more stable), (b) isomer 2, (c) isomer 3 and (d) isomer 4.

Furthermore, as shown in Table 3, the asymmetric stretching frequency of the carboxylate group (vas COO⁻) and the stretching frequency of the amide carbonyl group ($vC = O$, amide band) are shifted to the lower energy region (lower frequency) compared to the oxamic acid. These data suggest that both the amide group and the carboxylate group participate in the coordination. These experimental results are in agreement with theoretical calculations (Figure 3a) and with results of structure determination[1]. It is possible to observe that the frequency values are close to those observed for the sodium salt, which suggests a higher ionic character of the bonds in these complexes, a characteristic property of rare earth complexes[22].

3.4. PXRD

The X-ray diffractograms are presented in supplementary material (Figure S1). These results show that holmium and yttrium complexes were obtained with low degree of crystallinity. On the other hand, the complexes of Tb and

Figure 4. IR spectra of (a) oxamic acid, (b) sodium oxamate and of the complexes of: (c) Tb, (d) Dy, (e) Ho, (f) Er, (g) Tm, (h) Yb, (i) Lu, (j) Y and (l) Y theoretical.

Table 3. Main vibrational frequencies in infrared of the oxamate complexes of lanthanides and yttrium.

Assignments	Frequencies								
	Tb	Dy	Ho	Er	Tm	Yb	Lu	Y	Y*
ν O - H (H_2O)	$3394_{m,br}$	$3390_{m,br}$	$3213_{m,br}$	$3307_{m,br}$	$3208_{m,br}$	$3208_{m,br}$	$3220_{m,br}$	$3226_{m,\,al}$	
vas NH_2	overlapped	overlapped	overlapped	overlapped	3443_m	3442_m	3442_m	overlapped	3646, 3644, 3643
vs NH_2	overlapped	overlapped	overlapped	overlapped	3372_m	3376_m	3381_m	overlapped	3497, 3496, 3495
vas COO + δ_s NH_2	1702_{sh}	1701_{sh}	overlapped	overlapped	overlapped	overlapped	overlapped	overlapped	1758, 1738, 1737
ν C = O (CONH$_2$, Amide I band)	1638_{vs}	1638_{vs}	1639_{vs}	1641_{vs}	1633_{vs}	1661_{vs}	1653_{vs}	1638_{vs}	1699, 1686, 1683
δ_s NH_2	overlapped	overlapped	overlapped	overlapped	overlapped	overlapped	overlapped	overlapped	1567, 1566
δ_s NH_2 + ν C - N	1442_w	1447_w	1434_w	1452_w	1461_w	1427_w	1426_w	1437_w	1428, 1426, 1425
vs COO$^-$ + δ_s NH_2	1318_m	1320_m	1317_m	1342_m	1341_m, 1308_m	1342_m, 1310_m	1351_m, 1322_m	1318_m	1300, 1295, 1291
ρ NH_2 + ν C = O (amide) + ν C - N	1092_{vw}	1091_{vw}	1093_{vw}	1098_{vw}	1110_{vw}, 1091_{vw}	1110_{vw}, 1093_{vw}	1094_{vw}	1098_{vw}	1105, 1104, 1102

* theoretical; δ_s: symmetrical angular in plane deformation; ρ: asymmetric angular in plane deformation; L: oxamate; br: broad; vw: very week; w: week; m: medium; s: strong; vs: very strong.

Lu were obtained with high degree of crystallinity and the diffractograms for the complexes Tm, Yb and Lu suggest the formation of an isomorphous series.

4. Conclusion

The oxamates of heavy trivalent lanthanides and yttrium were synthesized and characterized by TG-DSC, vibrational spectroscopy in the infrared region (IR), elemental analysis, powder X-ray diffraction and EDTA complexometric titrations.

Based on the TG curves, elemental analysis and complexometric titration results, a general empirical formula could be established for the synthesized complexes as Ln(L)$_3$·nH$_2$O, in which Ln represents heavy trivalent lanthanides, L is oxamate and n = 1 (Dy, Ho, Y); 1.25 (Er); 1.5 (Tb and Lu); 2 (Tm) and 2.5 (Yb).

Simultaneous TG-DSC curves provided information about the thermal behavior of these complexes: dehydration, thermal stability and thermal decomposition steps.

The main gaseous products released during the thermal decomposition were identified as ammonia, hydrogen cyanide, nitrous oxides, CO$_2$ and CO.

The experimental and theoretical infrared spectroscopic data suggest that the oxamate acts as a chelating bidentate ligand to the metal ions through the oxygen of the amide and carboxylate groups. Furthermore, the great similarity

between the experimental infrared spectra for all the complexes suggests that all are coordinated in the same way.

5. Acknowledgements

6. References

1. Papadimitriou C, Veltsistas P, Marek J, Woollins JD. The preparation and X-ray structure of [Ho(oxam)$_3$(H$_2$O)$_3$]$_4$·2.75H$_2$O. *Inorganica Chimica Acta*. 1998;267(2):299-303.

2. Vansant C, Desseyn HO, Perlepes SP. The synthesis, spectroscopic and thermal study of oxamic acid compounds of some metal(II) ions. *Transition Metal Chemistry*. 1995;20(5):454-459.

3. Lazaridou V, Perlepes SP, Tsangaris JM. Synthesis, physical properties and spectroscopic studies of oxamato (- 1) lanthanide(III) complexes. *Journal of the Less Common Metals*. 1990;158(1):1-14.

4. Veltsistas PG, Christos PD, Karayannis MI. Synthesis and X-ray structure of an (oxamato)praseodymium polymer,

[Pr(HNCOCO$_2$)1.5(H$_2$O)$_3$]$_n$·2.75H$_2$O. *Polyhedron*. 1995;14(9):1251-1253.

5. Veltsistas PG, Papadimitriou CD, Slawin AMZ, Woollins JD. Synthesis, Characterization and X-Ray Structural Determination of the Nine-coordinate Tris-aqua Tetra-oxamato Neodymium(III) Complex [Nd(Hoxm)$_3$(H$_2$oxm)·2.5H$_2$O]$_n$. *Journal of Chemical Research, Synopses*. 1999;3:222-223.

6. Caires FJ, Lima LS, Gomes DJC, Gigante AC, Treu-Filho O, Ionashiro M. Thermal and spectroscopic studies of solid oxamate of light trivalent lanthanides. *Journal of Thermal Analysis and Calorimetry*. 2013;111(1):349-355.

7. Becke AD. Density-functional thermochemistry. III. The role of exact exchange. *The Journal of Chemical Physics*. 1993;98(7):5648.

8. Lee C, Yang W, Parr RG. Development of the Colic-Salvetti correlation-energy formula into a functional of the electron density. *Physical Review B*. 1988;37(2):785-789.

9. Treu-Filho O, Pinheiro JC, da Costa EB, Ferreira JEV, Figueiredo AF, Kondo RT, et al. Experimental and theoretical study of the compound [Pd(dmba)(NCO)(imz)]. *Journal of Molecular Structure*. 2007;829(1-3):195-201.

10. Filho OT, Pinheiro JC, Kondo RT. Designing Gaussian basis sets to the theoretical study of the piezoelectric effect of perovskite (BaTiO$_3$). *Journal of Molecular Structure: THEOCHEM*. 2004;671(1-3):71-75.

11. Treu Filho O, Pinheiro J, Kondo R, Marques RF, Paiva-Santos C, Davolos M, et al. Gaussian basis sets to the theoretical study of the electronic structure of perovskite (LaMnO$_3$). *Journal of Molecular Structure: THEOCHEM*. 2003;631(1-3):93-99.

12. Frisch MJ, Trucks GW, Schlegel HB, Scuseria GE, Robb MA, Cheeseman JR, et al. *Gaussian 09, Revision A.02*. Wallingford: Gaussian, Inc.; 2009.

13. Goodson D, Sarpal SK, Bopp P, Wolfsberg M. Influence on isotope effect calculations of the method of obtalnlng force constants from vibrational data. *The Journal of Physical Chemistry*. 1982;86(5):659-663.

14. Schelege HB. Some Practical Suggestions for Optimizing Geometries and Locating Transition States. In: Bertrán J, Csizmadia IG, eds. *New Theoretical Concepts for Understanding Organic Reactions*. Dordrecht: Springer; 1989. p. 33-53.

15. Dennington R, Keith T, Millam J. *GaussView, Version 5.0.8*. Shawnee Mission: Semichem Inc.; 2009.

16. Alves FS, Bembo LH, Caires FJ, Ionashiro EY. Thermoanalytical study of heavier trivalent lanthanides fumarates. *Journal of Thermal Analysis and Calorimetry*. 2013;113(2):739-744.

17. Caires FJ, Gigante AC, Gomes DJC, Treu-Filho O, Ionashiro M. Synthesis, thermal behavior and spectroscopic study of trivalentlanthanide and yttrium(III) α-hydroxyisobutyrates, in solid state. *Thermochimica Acta*. 2013;569:8-16.

18. Nunes WDG, Teixeira JA, do Nascimento ALCS, Caires FJ, Ionashiro EY, Ionashiro M. A comparative study on thermal behavior of solid-state light trivalent lanthanide isonicotinates in dynamic dry air and nitrogen atmospheres. *Journal of Thermal Analysis and Calorimetry*. 2016;125(1):397-405.

19. Locatelli JR, Ionashiro EY, Caires FJ, Carvalho CT. Synthesis, Characterization and Thermal Behavior of Solid-State Compounds of Light Trivalent Lanthanide Malonates. *Brazilian Journal of Thermal Analysis*. 2013;2(1):23-30.

20. Silverstein RM, Webster FX, Kiemle DJ. S*pectrometric identification of organic compounds*. 7th ed. Hoboken: Wiley; 2005. 512 p.

21. Nakamoto K. *Infrared and Raman spectra of inorganic and coordination compounds: Part A: Theory and Applications in Inorganic Chemistr*y. 6th ed. Hoboken: Wiley; 2009.

22. Bünzli JCG. On the design of highly luminescent lanthanide complexes. *Coordination Chemistry Reviews*. 2015;293-294:19-47.

Supplementary material

The following online material is available for this article:

Table S1. Selected optimized geometrical parameters for the yttrium complex in the ground state calculated at B3LYP levels.

Figure S1. X-ray powder diffraction patterns of the compounds: (a) Tb(L)$_3$·1.5H$_2$O, (b) Dy(L)$_3$·1H$_2$O, (c) Ho(L)$_3$·1H$_2$O, (d) Er(L)$_3$·1.25H$_2$O, (e) Tm(L)$_3$·2H$_2$O, (f) Yb(L)$_3$·2.5H$_2$O, (g) Lu(L)$_3$·1.5H$_2$O and (h) Y(L)$_3$·1H$_2$O.